Available online at www.sciencedirect.com
SCIENCE DIRECT®
Journal of Solid State Chemistry 177 (2004) 3660–3665
JOURNAL OF SOLID STATE CHEMISTRY
http://elsevier.com/locate/jssc

Defect and dopant properties of the Aurivillius phase $Bi_4Ti_3O_{12}$

Alan Snedden,[a] Philip Lightfoot,[a] Tim Dinges,[b] and M. Saiful Islam[b,*]

[a] School of Chemistry, University of St. Andrews, St. Andrews, Fife KY16 9ST, UK
[b] Materials Chemistry Group, Chemistry Division, University of Surrey, Guildford, Surrey GU2 5XH, UK

Received 24 March 2004; accepted 4 June 2004

Abstract

Computer modelling techniques have been used to investigate the defect and oxygen transport properties of the Aurivillius phase $Bi_4Ti_3O_{12}$. A range of cation dopant substitutions has been considered including the incorporation of trivalent ions (M^{3+} = Al, Ga and In). The substitution of In^{3+} onto the Bi site in the $[Bi_2O_2]$ layer is predicted to be the most favourable. The calculations suggest that lanthanide (Ln^{3+}) doping at the dilute limit preferentially occurs in the $[Bi_2O_2]$ layer, with probable distribution over both the $[Bi_2O_2]$ and the perovskite *A*-site at higher dopant levels. It is predicted that the reduction process involving Ti^{3+} and oxygen vacancy formation is energetically favourable. The energetics of oxide vacancy migration between various oxygen sites in the structure have been investigated.

Keywords: Aurivillius phase; Simulation; Ferroelectric; Layered perovskite; Oxide ion conduction

1. Introduction

The Aurivillius phases are a family of bismuth containing layered perovskites [1,2]. Their structure is based on a regular intergrowth of fluorite-like $[Bi_2O_2]^{2+}$ and perovskite-like $[A_{n-1}B_nO_{3n+1}]^{2-}$ layers, typical examples being Bi_2WO_6 ($n=1$), $SrBi_2Ta_2O_9$ ($n=2$) and $Bi_4Ti_3O_{12}$ ($n=3$). These materials have been widely studied as ferroelectrics since the early work of Smolenskii et al. [3] and Subbarao [4]. However, it is only more recently that the potential of these materials for commercial applications has begun to be realised. In particular, the discovery of low polarisation fatigue (i.e., negligible loss of remnant polarisation on repeated switching) in thin-film $SrBi_2Ta_2O_9$ [5], with consequent potential for uses in applications such as ferroelectric random access memories (FeRAMs), has renewed interest in the fundamental solid-state chemistry and physics of the Aurivillius phases. More recently, Park et al. [6] have shown that La-substituted $Bi_4Ti_3O_{12}$ thin films provide a promising alternative for FeRAM applications. In parallel with these developments, the discovery of high oxide ion conductivity in the so-called 'BIMEVOX' series of phases [7], derived from $Bi_4V_2O_{11}$ (an anion-deficient, $n=1$ Aurivillius phase) has also led to the search for similar behaviour in a range of related members of this family.

The aim of the present work is to apply atomistic simulation techniques, for the first time, to the study of the defect chemistry of the archetypal Aurivillius phase $Bi_4Ti_3O_{12}$. This model phase has been chosen as some of the more interesting developments in ferroelectricity within this family have been made on derivatives of this parent phase, prepared via either iso- or aliovalent cationic substitutions [8,9]. Specifically, doping of La^{3+} into the $Bi_4Ti_3O_{12}$ structure (Fig. 1) has recently been shown to produce excellent fatigue-free performance compared to the parent composition [6]. Also, prior work has reported the presence of promising oxide ion conductivity in $n=3$ and 4 Aurivillius phases via doping with aliovalent cations, e.g., M^{3+} (M = Al, Ga, In) for Ti^{4+} [10]. The conductivity is proposed to occur via a conventional hopping mechanism, requiring oxygen vacancies in the structure. However, a more recent powder X-ray diffraction study of the Ga^{3+}-doped phases concluded that the materials were impure [11], and contained a Bi_2O_3 impurity phase which may,

*Corresponding author. Fax: +44-1483-686851.
E-mail address: m.islam@surrey.ac.uk (M.S. Islam).

0022-4596/$ - see front matter © 2004 Elsevier Inc. All rights reserved.
doi:10.1016/j.jssc.2004.06.012

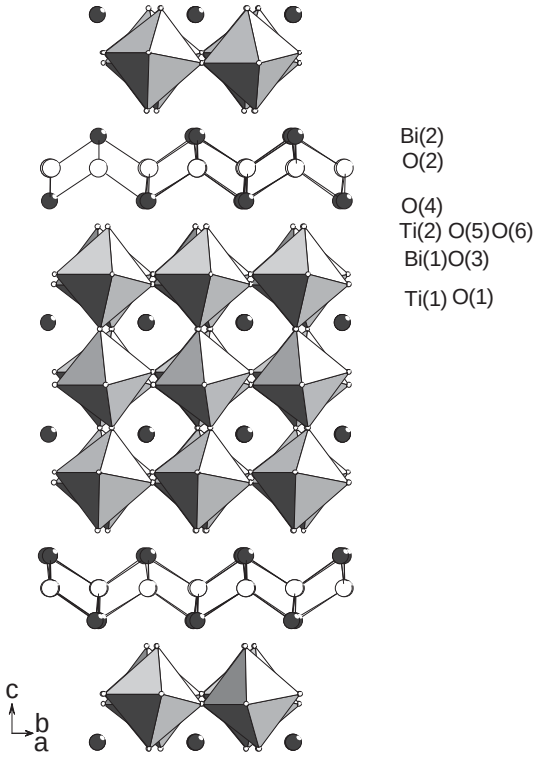

Fig. 1. $Bi_4Ti_3O_{12}$ structure, viewed along [110].

in part, be responsible for the observed ionic conductivity. The implication of this is that the tolerance of these phases to cation doping and/or oxide ion vacancies is much smaller than previously thought, which is a major focus of the present study.

The $Bi_4Ti_3O_{12}$ structure is relatively complex (Fig. 1), containing six crystallographically distinct oxygen sites and four different cation sites, viz. two distinct Ti sites (the '*B*' sites of the perovskite block) and two distinct Bi sites (the perovskite '*A*' site and the interlayer $[Bi_2O_2]$ site). It is of interest therefore to understand the nature and extent of the defect chemistry of $Bi_4Ti_3O_{12}$ using both experimental and modelling methods.

Atomistic simulation techniques are now established tools for the investigation of structures and energetics of complex materials. The techniques are well suited to modelling defect properties and ionic migration in oxide ion conductors, and have been applied successfully to perovskite [12–14] and brownmillerite phases [15]. In the context of related Aurivillius compounds, these methods have been used to study dopants and oxygen transport in $n = 1$ phases based on Bi_2WO_6 [16], and the crystal structures of a range of $n = 1-3$ phases [17]. The present work on the $n = 3$ Aurivillius phase $Bi_4Ti_3O_{12}$ will extend the previous computational studies to include dopant incorporation at all cation sites, and also the energetics of oxide ion vacancy migration.

2. Simulation methods

The simulations used in this study are based upon energy minimisation procedures, embodied in the GULP code [18]. The total energy of the system is given by a set of interatomic potentials that express the energy as a function of the atomic co-ordinates. For oxide materials the Born model is used, which divides the energies of the system into long-range Coulombic interactions, and a short-range term which describes the repulsions and van der Waals attractions between electron charge clouds. The form of the short-range term used is the Buckingham potential:

$$V(r) = Ae^{-r/\rho} - \frac{C}{r^6}. \quad (1)$$

It is also necessary to simulate ionic polarisation, for which the Dick–Overhauser shell model is used. In this model, the ion is described in terms of a core (representing the nucleus and core electrons) connected by a harmonic spring to a shell (representing the valence electrons). The shell model has been shown to simulate effectively both dielectric and elastic properties [18].

The defect calculations are performed using the Mott–Littleton approach, which involves partitioning the crystal lattice into two regions, so that the ions in the inner region are relaxed explicitly. The remainder of the crystal, in which the defect forces are relatively weak, is modelled using quasi-continuum methods.

Such simulation methods have been applied to the study of defects and oxide ion transport in a range of complex oxides [12–16]. As discussed previously [14,18], the validity of the model is assessed mainly by its ability to reproduce experimental crystal properties, which our model does for a complex structure. We stress that our simulations provide a useful guide and rationalisation of defect properties based on clear trends in the calculations at the atomic level.

3. Results and discussion

3.1. Structural modelling

The structure of $Bi_4Ti_3O_{12}$ was studied using the orthorhombic model (space group *B*2*cb*) suggested from powder neutron diffraction data [19]. This model has two sites containing Bi^{3+}, with different coordination environments (Fig. 1). The $[Bi_2O_2]$ layer site (Bi2) is an 8-coordinate position, whilst the perovskite *A*-site (Bi1) adopts 12-coordination. There are two Ti^{4+} containing sites, the perovskite *B*-sites, which are both distorted octahedral sites with the octahedra being rotated around the principal unit cell axes. It is these octahedral distortions, together with the co-operative displacement

of the Bi1 site, that are considered key to the ferroelectric properties of this family of materials.

The initial interatomic potentials were those derived by Pirovano et al. [17] to describe $n = 1$, 2 and 3 Aurivillius phases. Due to the importance of the octahedral distortions the effect of various Ti–O potentials on the calculated structural model was examined. To determine whether the model provided a good reproduction of the experimental data, the lattice parameters were examined. The result of these calculations is the final set of interatomic potentials used in the defect calculations given in Table 1. The calculated lattice parameters are listed in Table 2, which generally show good accord with the experimental data with an average difference of 1% for a relatively complex structure. This provides a valid starting point for the defect calculations.

3.2. Intrinsic defects

Calculations were first performed on the energies of isolated vacancy defects. The resulting energies are given in Table 3. Attempts to establish interstitial defect energies were unsuccessful, suggesting that such defects are not feasible, as expected. It is found that the oxygen (O2) position in the $[Bi_2O_2]$ layer is the lowest energy oxygen vacancy site. This is contrary to the hypothesis put forward previously [10], where the vacancies were proposed to create a brownmillerite-type sublattice.

Table 1
Interatomic potentials for $Bi_4Ti_3O_{12}$

	A (eV)	ρ (Å)	C (eV Å^6)
(a) Short-range Buckingham			
Bi–Bi	24244.50	0.3284	0
Bi–O	49529.35	0.2223	0
Ti–O	2549.4	0.2989	0
O–O	9547.96	0.2192	32
(b) Shell model			
Species	K(eV Å^2)	Shell(e)	
Bi^{3+}	359.55	−5.51	
Ti^{4+}	39.5	2.89	
O^{2-}	6.3	−2.04	

Table 2
Calculated and experimental lattice parameters for $Bi_4Ti_3O_{12}$

Parameter	Calculated	Experimental[a]
a (Å)	5.4474	5.4451(1)
b (Å)	5.4022	5.4101(1)
c (Å)	33.8184	32.8564(7)
$\alpha = \beta = \gamma$ (deg)	90	90
Lattice energy (eV)	−618.116	

[a] Values at 298 K Ref. [19].

Table 3
Calculated point defect energies of isolated vacancies

Ion site	Vacancy energy (eV)
Bi1	44.28
Bi2	55.24
Ti1	93.22
Ti2	96.71
O1	24.11
O2	15.35
O3	22.44
O4	18.61
O5	18.34
O6	18.57

There is no experimental evidence for this brownmillerite-related structure in $Bi_4Ti_3O_{12}$ and its derivatives.

Our results are consistent with X-ray photoelectron spectroscopy (XPS) studies of Jovalekic et al. [9], which suggest that the oxygen vacancies are sited close to bismuth ions, most probably in the $[Bi_2O_2]$ layer. Chemical intuition would also support the defect calculation in this respect, as the (O2) position is the most 'over-bonded' anion site in the Aurivillius phases in bond-valence terms; vacancy formation at this site would help to reduce the inherent stress in the lattice within this layer. In this context, dielectric studies of this system have probed relaxation phenomena, which are believed to be related to oxygen vacancy defects or local ion-jump mechanisms [8].

Many applications result in conditions where materials are expected to be used under a variety of oxygen partial pressures. Recent studies of Zhang et al. [9] have also suggested that the oxygen vacancy defect is the predominant factor determining ferroelectric fatigue. It is therefore desirable to examine the possibility of certain redox processes in the undoped material. In this system processes involving the reduction of the Ti^{4+} to Ti^{3+} have been examined via the following redox process:

$$O_o^x \rightarrow V_o^{\bullet\bullet} + \tfrac{1}{2}O_2 + 2e', \quad (2)$$

where V_o is an oxygen vacancy and e' is treated as a localised electronic species (Ti^{3+}). Our analysis has included all the key terms, but there are uncertainties in the absolute values due to the free-ion energies employed. Nevertheless, our concern here is to understand trends in the formation of electronic species; for this task our modelling methods have proved to be reliable.

Focussing on the most favourable oxygen vacancy (O2) and electronic terms, the energy for the reduction process is found to be highly favourable (−1.5 eV, Table 4). It is therefore predicted that $Bi_4Ti_3O_{12}$ may form Ti^{3+} and oxygen vacancies under reducing conditions (low oxygen pressures pO_2), which may lead to n-type conduction behaviour. Indeed, the presence of

Table 4
Calculated redox and oxygen vacancy migration energies

Process	Energy (eV)
Reduction reaction (2)[a]	−1.54
O1–O1 vacancy migration	2.52
O2–O2 vacancy migration	1.60

[a] Isolated electronic terms: $e'(-4.29\,\text{eV})$; $1/2\ O_2 - > O^{2-}(9.86\,\text{eV})$.

Ti^{3+} species and *n*-type conductivity is not unusual in other titanium-based oxides [20]. Since redox processes under reducing atmospheres have not been fully examined in $Bi_4Ti_3O_{12}$, this area requires detailed experimental investigation.

3.3. Dopant substitution

It has been demonstrated experimentally that the doping of lanthanide (Ln^{3+}) cations for Bi^{3+} in $Bi_4Ti_3O_{12}$ decreases the ferroelectric Curie temperature T_C [21]. It had originally been assumed that the lanthanide substitution occurred on the perovskite *A*-site (Bi1) and not on the $[Bi_2O_2]$ layer site (Bi2). However, recent powder X-ray diffraction studies [22,23] have shown that this is only an approximation, with La doping occurring on both sites for compositions $Bi_3LaTi_3O_{12}$ and $Bi_2La_2Ti_3O_{12}$. In fact, very recent electron diffraction and microscopy studies of Chu et al. [24] have suggested an even more complex defect mechanism in the $Bi_{4-x}La_xTi_3O_{12}$ system involving Bi/La cation disorder and lowering of symmetry.

In our present study, the approach to dopant incorporation involves the calculation of the Ln^{3+} dopant substitution energy at all the Bi^{3+} and Ti^{4+} sites, the latter with charge-compensating oxygen vacancies. The substitutions can be represented by the following defect reactions:

Ti-site:

$$\tfrac{1}{2}Ln_2O_3 + Ti_{Ti}^{x} = Ln'_{Ti} + TiO_2 + \tfrac{1}{2}V_O^{\bullet\bullet}. \quad (3)$$

Bi-site:

$$\tfrac{1}{2}Ln_2O_3 + Bi_{Bi}^{x} = Ln_{Bi}^{x} + \tfrac{1}{2}Bi_2O_3. \quad (4)$$

The energies of these 'solution' reactions can then be calculated by combining the appropriate defect and lattice energy terms. Using this consistent approach creates a guide to the relative energies for different dopant ions on different lattice sites. The calculated solution energies for lanthanide (Ln^{3+}) dopants are plotted against ion size in Fig. 2.

Examination of these results reveals two main points. First, the doping of the lanthanide cations into either of the Ti^{4+} sites is highly unfavourable as expected, which we show explicitly on energetic grounds. This accords well with experimental data, since the Ln^{3+} cations are viewed as too large to occupy the octahedral site.

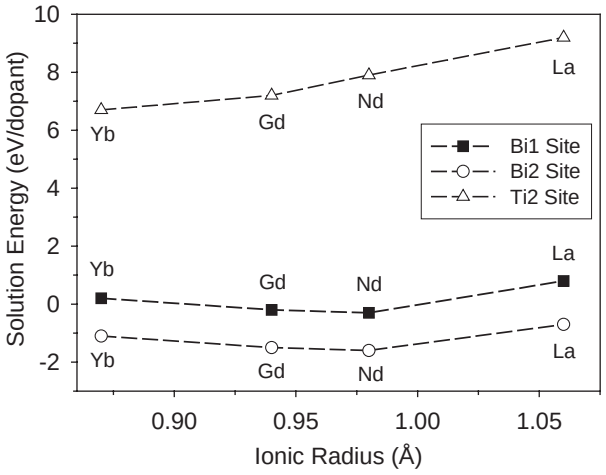

Fig. 2. Calculated solution energies as a function of ionic radius for lanthanide (Ln^{3+}) dopants at Bi and Ti sites (only Ti2 is shown, as it is the lower energy Ti site).

Second, the solution energies obtained for the two Bi^{3+} sites suggest that the $[Bi_2O_2]$ layer site is slightly favoured over the perovskite *A*-site. Moreover, the solution energies for the lanthanide cations show no significant trend with cation size. X-ray powder diffraction studies [22,23] show a strong preference for Ln^{3+} substitution at the Bi1 site, which increases with decreasing Ln^{3+} cation size.

In these simulations only an isolated dopant ion is inserted, i.e., the calculation takes place at the dilute limit. The simulation result does not suggest that doping will take place only on the $[Bi_2O_2]$ layer site, but that the initial doping will occur on that site. Nevertheless, in view of the large lattice energies used in the calculations, the very small difference in the solution energies for the two Bi^{3+} sites may suggest that doping would occur over both sites at higher concentrations, with cation disorder over the two sites.

Similar calculations were performed for the smaller trivalent cations, Al, Ga and In. The results are again displayed as a plot of solution energy versus ionic radius (Fig. 3). These results show that both Ti^{4+} sites are unfavourable for the incorporation of these M^{3+} dopants. The most favourable substitution site for the M^{3+} dopants is Bi2, although Ga^{3+} has a relatively high solution energy suggesting lower solubility. It is worth noting that recent X-ray powder diffraction studies [11] of related Ga^{3+}-doped phases concluded that the limit of solid solubility for Ga^{3+} is much smaller than previously thought. The lowest solution energy is predicted for In^{3+} doping, which we suggest warrants further experimental work.

3.4. Oxide ion migration

The M^{3+}-doped phases have been proposed as oxide ion conductors [10]. For example, conductivity data for

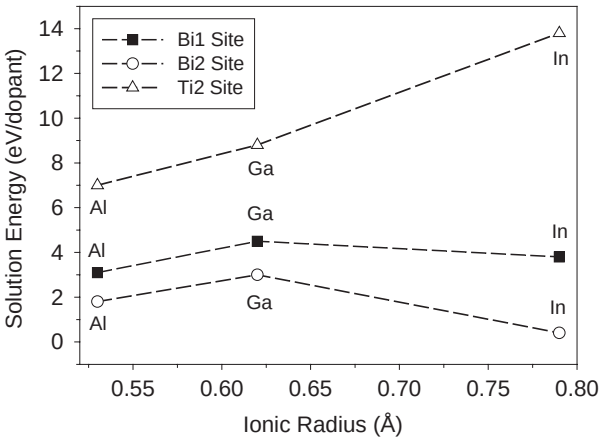

Fig. 3. Calculated solution energies as a function of ionic radius for trivalent (M^{3+}) dopants at Bi and Ti sites (only Ti2 is shown, as it is the lower energy Ti site).

the 3-layer Aurivillius phases find activation energies of 0.62 eV above 775°C and 1.28 eV below 775°C for the $Bi_2Sr_2Nb_2GaO_{11.5}$ system, and values for $Bi_2Sr_2Nb_2AlO_{11.5}$ of 0.61 eV and 1.26 eV, above and below 800°C, respectively [10]. However, it has been postulated that any high oxide ion conductivity could, at least in part, be influenced by the presence of a Bi_2O_3 impurity phase [11]. The Bi_2O_3 phases are known to have activation energies for oxygen ion transport of about 0.4–0.8 eV depending upon the structure type and dopant level [7].

Simulation studies can greatly enhance our understanding of this problem by evaluating the activation energies for various defect migration mechanisms at the atomic level. We have therefore examined the energetics of oxygen vacancy migration in $Bi_4Ti_3O_{12}$. The migration energies were evaluated from energy profiles by calculating the energy of the migrating anion along the diffusion path between adjacent oxygen sites. In this way, the 'saddle-point' configuration can be identified, from which the energy barrier to migration is derived.

Calculations were performed for the $[Bi_2O_2]$ oxygen site (O2) as the lowest energy oxygen vacancy site, and the O1 position in the inner Ti1–O1 plane. It was found that the activation energies for O1 and O2 vacancy migration are relatively high values of 2.5 and 1.6 eV, respectively (Table 4). Such large migration energies for $Bi_4Ti_3O_{12}$ suggest that high oxide ion conductivity would not be exhibited in this phase.

Recent dielectric and mechano-elastic measurements of Jimenez et al. [25] on point defects in $Bi_4Ti_3O_{12}$ find relaxation peaks that are attributed to oxygen vacancy migration ($E_a = 1.90$ eV at $T = 450$°C). Elastic relaxation peaks are also present close to 300°C whose activation energy (1.50 eV) and characteristic time (10^{-15} s) suggest a vacancy migration process, which are consistent with our calculations.

In a previous simulation study [17], phases based on doped Bi_2WO_6 ($n = 1$) were found to have activation energies as low as 0.63 eV for oxide vacancy migration, in accord with conductivity studies. In general, the order of magnitude of oxide ion conductivity is significantly lower in the $n > 1$ Aurivillius phases than in the $n = 1$ BIMEVOX compounds based on doped $Bi_4V_2O_{11}$ (7). Baux et al. [26] have discussed the lower ionic conductivity and higher activation energies (>1.2 eV) found in the $n > 1$ Aurivillius phases in comparison to the doped Bi_2WO_6 ($n = 1$) material; they rationalised this in terms of the structural differences and the role of the Bi^{3+} lone pair in the migration mechanism of oxygen vacancies. One of the aims of our present study is to encourage further experimental work to (re)examine the case for low oxide ion conductivity in $n > 1$ Aurivillius phases.

4. Conclusion

Atomistic simulation techniques have been employed to investigate the defect, dopant and oxygen transport properties of the 3-layer Aurivillius phase $Bi_4Ti_3O_{12}$ that are relevant to potential ferroelectric applications. The following main points emerge.

(1) Investigations into Ln^{3+} doping (Yb, Gd, Nd, La) have suggested that incorporation could occur at both of the Bi^{3+} sites as observed experimentally. At the dilute limit a slight energetic preference for the $[Bi_2O_2]$ layer site is found.
(2) Calculations performed on the smaller M^{3+} dopants (Al, Ga, In) have suggested that substitution is unlikely to occur at any of the perovskite sites (Bi1, Ti1 or Ti2) on energetic grounds. For substitution at the $[Bi_2O_2]$ site, In^{3+} is predicted to be the most favourable dopant, which merits further experimental investigation.
(3) The favourable reduction energy suggests the formation of Ti^{3+} and oxygen vacancies under reducing atmospheres (low pO_2), which could lead to *n*-type conduction behaviour. Oxygen vacancy migration has been examined with the calculation of high activation barriers (>1.6 eV), suggesting that high oxide ion conductivity is unlikely to be exhibited in the $Bi_4Ti_3O_{12}$ phase.

Acknowledgments

We thank the EPSRC for a studentship for A. Snedden and the EPSRC Perovskite Network for funding an interlaboratory exchange. The supercomputer facilities at the Rutherford-Appleton Laboratory

was used for the simulations. We also thank Drs. J.R. Tolchard and R.A. Davies for helpful discussions.

References

[1] B. Aurivillius, Ark. Kemi. 1 (1949) 463.
[2] B. Frit, J.P. Mercurio, J. Alloys Compds. 188 (1992) 27.
[3] G.A. Smolenskii, V.A. Isupov, A.I. Agranovskaya, Sov. Phys.—Solid State 3 (1961) 651.
[4] E.C. Subbarao, J. Phys. Chem. Solids 23 (1962) 665.
[5] C.A.-P. de Araujo, J.D. Cuchiaro, L.D. McMillan, M.C. Scott, J.F. Scott, Nature 374 (1995) 627.
[6] B.H. Park, B.S. Kang, S.D. Bu, T.W. Noh, J. Lee, W. Jo, Nature 410 (1999) 682.
[7] (a) F. Abraham, J.C. Boivin, G. Mairesse, G. Nowogrocki, Solid State Ion. 40-1 (1990) 943;
(b) J.C. Boivin, G. Mairesse, Chem. Mater. 10 (1998) 2870;
(c) I. Abrahams, F. Krok, J. Mater. Chem. 12 (2002) 3551;
(d) S. Nakayama, Ceram. Int. 28 (2002) 907.
[8] (a) H.S. Shulman, D. Damjanaovic, N. Setter, J. Am. Ceram. Soc. 83 (2000) 528;
(b) S. Luo, Y. Noguchi, M. Miyayama, T. Kudo, Mater. Res. Bull. 36 (2001) 531;
(c) Y.Y. Yao, C.H. Song, P. Bao, D. Su, X.M. Lu, J.S. Zhu, Y.N. Wang, J. Appl. Phys. 95 (2004) 3126.
[9] (a) C. Jovalekic, M. Pavlovic, P. Osmokrovic, L.J. Atanasoka, Appl. Phys. Lett. 72 (1998) 1051;
(b) S.T. Zhang, Y.F. Chen, J. Wang, G.X. Cheng, Z.G. Liu, N.B. Ming, Appl. Phys. Lett. 84 (2004) 3660;
(c) Q.D. Zhou, B.J. Kennedy, C.J. Howard, Chem. Mater. 15 (2003) 5025;
(d) D.Y. Suarez, I.M. Reaney, W.E. Lee, J. Mater. Res. 16 (2001) 3139.
[10] (a) K.R. Kendall, J.K. Thomas, H.-C. zur Loye, Solid State Ion. 70/71 (1994) 221;
(b) J.K. Thomas, K.R. Kendall, H.-C. zur Loye, Solid State Ion. 70/71 (1994) 225;
(c) K.R. Kendall, J.K. Thomas, H.-C. zur Loye, Chem. Mater 7 (1995) 50.
[11] A. Snedden, S.M. Blake, P. Lightfoot, Solid State Ion. 156 (2003) 439.
[12] (a) R.A. Davies, M.S. Islam, J.D. Gale, Solid State Ion. 126 (1999) 323;
(b) M.S. Islam, R.A. Davies, J.D. Gale, Chem. Commun (2001) 661.
[13] M.S. Islam, R.A. Davies, J. Mater. Chem. 14 (2004) 86.
[14] (a) M.S. Islam, J. Mater. Chem. 10 (2000) 1027;
(b) M.S. Islam, Solid State Ion. 154–155 (2002) 75.
[15] C.A.J. Fisher, M.S. Islam, Solid State Ion. 118 (1999) 355.
[16] M.S. Islam, S. Lazure, R.-N. Vannier, G. Nowogrocki, G. Mairesse, J. Mater. Chem. 8 (1998) 655.
[17] C. Pirovano, M.S. Islam, R.-N. Vannier, G. Nowogrocki, G. Mairesse, Solid State Ion. 140 (2001) 115.
[18] J.D. Gale, J. Chem. Soc. Faraday Trans. 93 (1997) 629.
[19] P. Lightfoot, C.H. Hervoches, Proceedings of CIMTEC, 10th International Ceramics Congress, Florence, Italy, July 2002.
[20] (a) D.M. Smyth, Solid State Ion. 129 (2000) 5;
(b) P. Knauth, H.L. Tuller, J. Appl. Phys. 85 (1999) 897.
[21] R.W. Wolfe, R.E. Newnham, J. Electrochem. Soc.: Solid State Ion. 116 (1969) 832.
[22] C.H. Hervoches, P. Lightfoot, J. Solid State Chem. 153 (2000) 66.
[23] N.C. Hyatt, J.A. Hriljac, T.P. Comyn, Mater. Res. Bull. 38 (2003) 837.
[24] M.-W. Chu, M.-T. Caldes, L. Brohan, M. Ganne, A.-M. Marie, O. Joubert, Y. Piffard, Chem. Mater. 16 (2004) 31.
[25] B. Jimenez, R. Jimenez, A. Castro, P. Millan, L. Pardo, J. Phys.: Condens. Matter. 13 (2001) 7315.
[26] N. Baux, R.N. Vannier, G. Mairesse, G. Nowogrocki, Solid State Ion. 91 (1996) 243.